IET Smart Grid

Research Article

IET Journals
The Institution of Engineering and Technology

Distributed, fixed-time, and bounded control for secondary voltage and frequency restoration in islanded microgrids

eISSN 2515-2947
Received on 11th July 2018
Revised 17th December 2018
Accepted on 21st February 2019
E-First on 1st April 2019
doi: 10.1049/iet-stg.2018.0115
www.ietdl.org

Sonam Shrivastava[1], Bidyadhar Subudhi[1] ✉

[1]*Centre for Renewable Energy Systems, Dept. of Electrical Engineering, National Institute of Technology Rourkela, Rourkela-769008, India*
✉ *E-mail: bidyadhar@nitrkl.ac.in*

Abstract: Microgrid (MG) technology evolves as a promising solution to deal with the intermittent renewable generations and frequently changing load demand. This paper proposes a fully distributed and bounded secondary control algorithm with flexible convergence time for voltage and frequency restoration. It also enables accurate active power sharing for an islanded MG, compared with the well-known consensus-based distributed control approach. The proposed control scheme achieves accelerated fixed-time convergence. The upper bound on the convergence is established by using the Lyapunov stability theory. The bounded, distributed control approach restores the voltage and frequency in fixed-time while sharing the active power precisely. Further, the proposed controller is adaptive to the communication topology change and supports the plug and play feature of MG. Extensive simulations have been pursued using MATLAB/SimPowerSyetem toolbox considering frequent load perturbation and communication topology change. The obtained results are analysed to verify the performance of the proposed control algorithm. It is observed that the proposed bounded input controller converges faster than the conventional method.

1 Introduction

Utilisation of Renewable Energy Sources (RES) in place of fossil fuel is a feasible solution for combating growing environmental pollution [1]. These RES as distributed generators (DG), storage devices, and local loads together form a modern small-scale power system known as microgrid (MG) [2]. MG is reliable and flexible than the conventional grid and can operate in both grid-tied and islanded modes. In grid-tied mode, utility grid maintains the demand-supply balance and provides voltage and frequency support. Scheduled maintenance or spontaneously occurred fault results in isolation of MG from the utility grid [3]. The islanded MG with intermittent RES, and low inertia necessitates an appropriate control design for its seamless and stable operation.

When islanded, power-sharing, frequency, and voltage stability of MG are disoriented [4]. The control objectives such as voltage and frequency restoration under any operating condition and accurate power-sharing in islanded mode are realised by adapting a hierarchical control structure [5, 6]. This three-layer hierarchical control scheme consists of primary, secondary, and tertiary control levels. The primary control level is locally implemented at each DG terminal via $P-f$ and $Q-V$ droop schemes in a distributed manner. Regardless of flexible and simple operation, droop control leads to voltage and frequency deviation from nominal values in steady state. The secondary control is often used to restore the voltage and frequency to their nominal values [7]. The tertiary control deals with the power flow and cost optimisation.

For secondary control, centralised and distributed structures have been reported in literature [8–10]. A centralised control structure necessitates a complex communication network and a central computing unit, that are costly and unreliable. Further, it suffers from risk of single-point-failure [11]. Alternatively, a multi-agent-system (MAS)-based distributed secondary control structure is introduced to solve the frequency, voltage, and power regulation problem in MG network [12–17]. In [12, 13], a feedback linearisation control scheme is employed to convert the secondary frequency control into a tracking synchronisation problem; where the convergence is achieved asymptotically using the neighbourhood tracking error-based method. Further, the controller performance depends on the MG system parameters. In [14], a fully distributed controller is proposed to deal with the trade-off between voltage restoration and reactive power sharing, whereas the frequency restoration is ignored. A distributed network control approach is presented in [15], which requires the average voltage and frequency information to be shared with the local controller of each DG unit and is similar to the centralised control structure. A droop-free distributed control approach is presented in [16], where the absence of droop scheme makes the system vulnerable to communication network failure. An exponential fast asymptotic control approach based on dynamic average consensus algorithm is presented in [17] for voltage and frequency restoration. The controller is designed using a single integrator dynamics of DG unit, and the upper bound on convergence time is not defined. Hence, this control approach is not suitable for fast changing operating conditions.

The existing distributed secondary control approaches converge asymptotically, hence are not suitable for high RES penetration, sudden load perturbations, and fast-changing operation. Flexible fixed-time secondary control approaches with accelerated convergence rate are desirable for stable MG operation. Recently, several finite-time control approaches are reported in literature [18–23]. A finite-time frequency control scheme is presented in [18], which uses a complex communication network, and it did not discuss the voltage and power regulation. Reference [19] proposes a finite-time frequency restoration control approach based on consensus algorithm. Following this line, finite-time voltage control approaches are reported in [20, 21], but both adopt asymptotic control approach for frequency and active power regulation. Reference [24] presents a finite-time control approach for voltage, frequency, and active power regulation, but unable to establish upper bound for the restoration time.

However, among the available finite-time approaches, a controller with bounded input constraint is rarely practiced. In [25], a saturation function is used in finite-time frequency controller design to limit the control input within bound, but the voltage control method has asymptotic convergence. Similarly, [26] also provides a bounded control input only for frequency and active power regulation.

A controller with bounded input constraint is worth investigation ascertaining its suitability for practical applications and fast-changing operating conditions. Here, three basic requirements of distributed secondary control namely: (i) restoration of voltage and frequency in finite-time; (ii) precise active power sharing; and (iii) independent from MG system

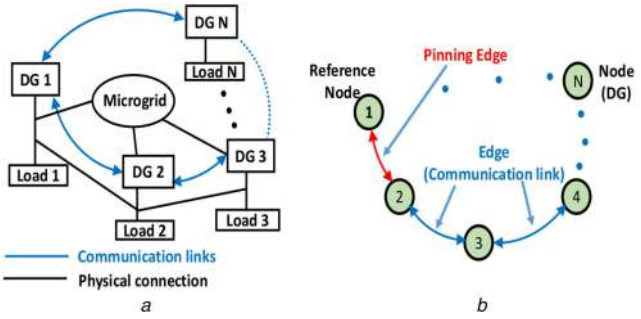

Fig. 1 *Microgid networked model*
(a) Physical network of DG units,
(b) Information sharing over communication network

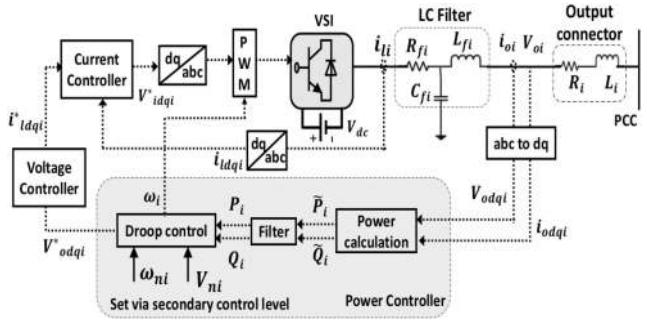

Fig. 2 *Block diagram of inverter-based* ith *DG unit*

parameters are considered. This paper proposes a distributed bounded and fixed-time control approach for voltage, frequency, and active power regulation. The contributions of the paper are as follows.

- In comparison with the asymptotic control approaches reported in [12–17], and the finite-time control approaches with unbounded control inputs in [18–22], here we proposed a fixed-time control schemes for voltage and frequency restoration and accurate power-sharing. The designed control schemes are augmented with constrained control input to suppress the transient overshoot. Unlike the centralised control structure, the proposed control schemes are fully distributed and necessitate only neighbour information. This enables the use of a cost-efficient sparse communication network and performs well even when only one DG has access to the reference value in the MG network. The stability proofs and upper bound on the convergence time are presented via Lyapunov techniques. The convergence time can be tuned according to user demand and operating condition using the controller gains and it only depends on the connectivity of communication network. Also, the proposed control approaches are independent of parameters of MG system. In comparison with the existing distributed controllers in [12, 13], the proposed controller achieve consensus rapidly and exhibits faster convergence performance for controller activation and sudden load perturbation.

The organisation of the paper is summarised as follows. Section 2 gives the brief introduction to the graph theory, primary control of inverter-based DG, and fixed-time secondary control. Section 3 presents the proposed distributed, bounded, fixed-time secondary control algorithms for voltage frequency, and active power regulation, and the convergence proofs. Section 4 presents simulation of the proposed control scheme for different situations such e.g. load perturbation and communication topology change together with the analysis of the results. Section 5 concludes the paper.

2 Preliminaries

Fig. 1 shows the networked multi-agent-based MG framework that incorporates the both physical inverter-based DG units and cyber network for information sharing. The cyber network can be considered as an undirected communication network and modelled as a weighted undirected graph.

2.1 Graph theory

The cyber-network can be modelled as a weighted undirected graph $G = (v, \varepsilon, \mathscr{A})$ with a set of nodes (DGs) $v = (v_1, v_2, \ldots v_N)$, a set of edges (communication links) $\varepsilon = \{e_1, e_2, \ldots, e_N\}$, $\varepsilon \subset v \times v$, and a weighted adjacency matrix $\mathscr{A} = [a_{ij}]_{N\times N}$, with $a_{ii} = 0$, $a_{ij} = a_{ji} = 1$ if $(v_i, v_j) \in \varepsilon$, $(v_j, v_i) \in \varepsilon$. The set of neighbours of ith DG is given as $\mathscr{N}_i = \{j | (v_j, v_i) \in \varepsilon\}$. The in-degree matrix is defined as $D = \text{diag}\{d_i\}$, with d_i is number of incoming links at ith node i.e. $d_i = \sum_{j\in\mathscr{N}_i} a_{ij}$. The Laplacian matrix is defined as $\mathscr{L} = D - \mathscr{A}$. It is assumed that at least one DG has access to the reference values i.e. $g_i > 0$ for ith DG. A graph has a spanning tree if there is at least one directed path from the reference node to every other node in the graph. The eigen value of Laplacian matrix $\mathscr{L}$ satisfy $0 = \lambda_1 < \lambda_2 \leq \cdots \leq \lambda_N$.

2.2 Primary control

Consider a MG with N inverter-based DG units. Fig. 2 shows the configuration of ith DG unit in islanded operating mode. Each DG unit contains a DC energy source, a DC/AC inverter, an LC filter, and a resister-inductor (RL) output connecter. Each DG's non-linear dynamics are modelled using the synchronously rotating $d-q$ frame converted to the common reference frame with angular frequency ω_{ref} as the common reference frame frequency [27]. The pulse width modulator (PWM) block in the primary control comprises of three loops namely current control loop, voltage control loop, and power control loop. These control loops generate the input signal to control the gating pulse of the inverter. Primary control is implemented in the power control loop with nominal set points V_{ni}, and ω_{ni}, set up by the secondary control level. The droop control scheme mimics the behaviour of synchronous generator, and the frequency and voltage droop characteristic for an inductive line can be given as [27],

$$\omega_i = \omega_{ni} - k_{Pi}^{\omega} P_i \tag{1}$$

$$V_i = V_{ni} - k_{Qi}^{V} Q_i \tag{2}$$

where ω_{ni} and V_{ni} are primary frequency and voltage control references, set by secondary control level. P_i and Q_i are active and reactive power of ith DG, k_{Pi}^{ω} and k_{Qi}^{V} are frequency and voltage droop gains, respectively. The output voltage magnitude $V_i = \sqrt{V_{odi} + V_{oqi}}$ with V_{odi} and V_{oqi} are d-axis and q-axis voltage components. The primary control strategy enables the alignment of direct component of output voltage magnitude on d-axis of reference frame and makes quadrature component zero i.e. $V_{oqi} = 0$ and $V_{odi} = V_i$.

2.3 Fixed-time secondary control

Despite the simple implementation and distributed structure, there might be voltage magnitude and frequency deviations in the droop control scheme. The secondary control level is employed to eliminate these deviations. Distributed secondary control updates the primary control set points via the control laws designed based on local and neighbours' information shared over a sparse communication network. In asymptotic approaches of distributed secondary control, the convergence time is unknown and the consensus is achieved over an infinite-time horizon, whereas in the fixed-time approach, the convergence time is greatly reduced which is desirable in fast operations. Furthermore, the fixed-time control objective can be expressed as follows.

1. Simply implementing the frequency restoration control law leads to inaccurate active power sharing, thus, for fixed-time frequency and active power regulation,

$$\begin{cases} \lim\limits_{t \to T_f} \left(\omega_i(t) - \omega_j(t)\right) = 0 \\ \omega_i(t) = \omega_j(t) = \omega_{\text{ref}} \end{cases}, \quad \forall t \geq T_f, \forall i, j \in N \cdot \quad (3)$$

$$\begin{cases} \lim\limits_{t \to T_f} \left(k_{Pi}^{\omega} P_i - k_{Pj}^{\omega} P_j\right) = 0 \\ k_{Pi}^{\omega} P_i = k_{Pj}^{\omega} P_j \end{cases}, \quad \forall t \geq T_P, \forall i, j \in N \cdot \quad (4)$$

where T_f is the frequency restoration time, and T_P is the active power regulation time for the proposed bounded secondary control. The restoration time for frequency and active power regulation is given by

$$T_F = \max\left\{T_f, T_P\right\} \cdot \quad (5)$$

2. Considering line impedance effect of electrical network, voltage restoration, and reactive power sharing objectives cannot be solved together. Therefore, for the fixed-time voltage regulation,

$$\begin{cases} \lim\limits_{t \to T_V} \left(V_i(t) - V_j(t)\right) = 0 \\ V_i(t) = V_j(t) = V_{\text{ref}} \end{cases}, \quad \forall t \geq T_V, \forall i, j \in N \cdot \quad (6)$$

where T_V is the voltage restoration time for the proposed bounded secondary control.

Now, the control input ω_{ni} and V_{ni} are designed to achieve the control goals (3), (4), and (6) by using input/output feedback linearisation. The secondary control problem can be considered as the tracking synchronisation problem with a leader DG has access to the reference value. Differentiating (1) and (2), with respect to time yields,

$$\dot{\omega}_i = \dot{\omega}_{ni} - k_{Pi}^{\omega} \dot{P}_i \equiv \xi_i^{\omega} \quad (7)$$

$$\dot{V}_i = \dot{V}_{ni} - k_{Qi}^{V} \dot{Q}_i \equiv \xi_i^{V} \quad (8)$$

where ξ_i^{ω} and ξ_i^{V} are the auxiliary control inputs for frequency and voltage, respectively. For accurate power-sharing consider $k_{Pi}^{\omega} \dot{P}_i = \xi_i^{P}$, then, $\xi_i^{\omega} = \dot{\omega}_i = \dot{\omega}_{ni} - \xi_i^{P}$ and $\xi_i^{V} = \dot{V}_i = \dot{V}_{ni} - k_{Qi}^{V} \dot{Q}_i$. The primary frequency and voltage set points i.e. V_{ni} and ω_{ni} are given as

$$\omega_{ni} = \int \left(\xi_i^{\omega} + \xi_i^{P}\right) \mathrm{d}t \cdot \quad (9)$$

$$V_{ni} = \int \left(\xi_i^{V} + k_{Pi}^{\omega} \dot{Q}_i\right) \mathrm{d}t \cdot \quad (10)$$

We present the following Lemmas to propose the main results.

Lemma 1: Let $a_{ij} = a_{ji}$, and y is an odd function, then [28],

$$\sum_{i=1}^{n} \sum_{j=1}^{n} a_{ij} x_i y\left(x_i - x_j\right) = \frac{1}{2} \sum_{i=1}^{n} \sum_{j=1}^{n} a_{ij} \left(x_i - x_j\right) \times y\left(x_i - x_j\right) \cdot \quad (11)$$

Lemma 2: If G is an undirected graph with spanning tree. Then, for the Laplacian matrix $\mathscr{L}$ following are true [29],

1. $x^T \mathscr{L} x = (1/2) \sum_{i,j=1}^{n} a_{ij} \left(x_j - x_i\right)^2$ and the Laplacian $\mathscr{L}$ is positive semi-definite i.e. all the eigen values have positive real parts.
2. The algebraic connectivity or the second smallest eigenvalue of $\mathscr{L}$ is defined as $\lambda_2(\mathscr{L})$, then one has $x^T \mathscr{L} x \geq \lambda_2(\mathscr{L}) x^T x$, if $1^T x = 0$.

Lemma 3: For an undirected graph G, matrix $(\mathscr{L} + G)$ is positive definite and holds [29],

1. $x^T(\mathscr{L} + G)x = (1/2) \sum_{i,j=1}^{N} a_{ij} \left(x_j - x_i\right)^2 + \sum_{i=1}^{N} g_i x_i^2$.
2. The smallest eigenvalue of $(\mathscr{L} + G)$ is defined as $\lambda_1(\mathscr{L} + G)$, then one has $x^T(\mathscr{L} + G)x \geq \lambda_1(\mathscr{L} + G)x^T$.

Lemma 4: Consider a continuous system $\dot{x} = y(x)$ with $y(0) = 0$. Assume, there exists a positive definite function $V(x): [0, \infty) \to [0, \infty)$, then $V(x) \leq -l_1 V(x)^{l_2}$, with $l_1 > 0$, and $0 < l_2 < 1$. $V(x)$ reaches to zero in fixed settling time [30],

$$T \leq \frac{V(0)^{1 - l_2}}{l_1 (1 - l_2)} \cdot \quad (12)$$

3 Distributed, fixed-time, and bounded secondary control

In the section, a distributed, fixed-time secondary control scheme for voltage, frequency, and active power regulation are designed with constrained input.

3.1 Frequency and active power regulation

The droop control scheme stabilises the voltage and frequency after islanding but they are not necessarily the nominal values. The auxiliary distributed fixed-time secondary frequency restoration scheme with a bounded control input ξ_i^{ω} is designed as

$$\xi_i^{\omega} = C_{\omega i} \left(\sum_{j \in \mathscr{N}_i} \alpha_{\omega} a_{ij} \text{sig}\left(\omega_j - \omega_i\right)^{m/n} + \beta_{\omega} g_i \text{sig}\left(\omega_{\text{ref}} - \omega_i\right)^{m/n} \right) \quad (13)$$

where $C_{\omega i}$ is positive gain satisfying following inequality

$$0 < C_{\omega i} \leq \frac{B_{\omega i}}{|g_i| + \sum_{j \in \mathscr{N}_i} |a_{ij}|} \quad (14)$$

with $B_{\omega i} > 0$ is the upper bound of the control input ξ_i^{ω}; $\mathscr{N}_i$ is the set of neighbours; ω_{ref} is the angular frequency reference; m, n are odd positive integers with $m < n$, and α_{ω}, β_{ω} are coupling gains; g_i is the weight of pinning gain, i.e. the weight of the edge which has direct access to the reference node; $\text{sig}(x)^a = \text{sgn}(x)|x|^a$; $\text{sgn}(\cdot)$ defines Signum function. Further, implementing only the secondary fixed-time frequency restoration scheme may result in inaccurate active power sharing. Therefore, the auxiliary active power sharing control input ξ_i^{P} is designed as

$$\xi_i^{P} = C_{Pi} \left(\sum_{j \in \mathscr{N}_i} \alpha_P a_{ij} \text{sig}\left(k_{Pj}^{\omega} P_j - k_{Pi}^{\omega} P_i\right)^{m/n} \right) \quad (15)$$

where C_{Pi} is positive gain satisfying following inequality

$$0 < C_{Pi} \leq \frac{B_{Pi}}{\sum_{j \in \mathscr{N}_i} |a_{ij}|} \quad (16)$$

with $B_{Pi} > 0$ is the upper bound of the control input ξ_i^{P}; α_P is the coupling gain.

Defining the frequency and active power error as $\delta_{\omega i} = \omega_i - \omega_{\text{ref}}$, and $\delta_{Pi} = k_{Pi}^{\omega} P_i - (1/N) \sum_{i=1}^{N} k_{Pi}^{\omega} P_i$. Then, $\dot{\delta}_{\omega i} = \dot{\omega}_i$ and $\dot{\delta}_{Pi} = k_{Pi}^{\omega} \dot{P}_i$. Since $(1/N) \sum_{i=1}^{N} k_{Pi}^{\omega} \dot{P}_i = 0$ for an undirected network, $(1/N) \sum_{i=1}^{N} k_{Pi}^{\omega} P_i$ is time invariant. From (7) and (8), we

have $\dot{\delta}_{\omega i} = \dot{\omega}_i = \xi_i^{\omega}$ and $\dot{\delta}_{Pi} = k_{Pi}^{\omega}\dot{P}_i = \xi_i^{P}$. The control inputs in (13) and (15) can be modified as

$$\xi_i^{\omega} = \dot{\delta}_{\omega i} = C_{\omega i}\Bigg(\sum_{j\in\mathcal{N}_i}\alpha_{\omega}a_{ij}\mathrm{sig}\big(\delta_{\omega j}-\delta_{\omega i}\big)^{m/n} - \beta_{\omega}g_i\mathrm{sig}(\delta_{\omega i})^{m/n}\Bigg)\cdot \tag{17}$$

and

$$\xi_i^{P} = \dot{\delta}_{Pi} = C_{Pi}\Bigg(\sum_{j\in\mathcal{N}_i}\alpha_{P}a_{ij}\mathrm{sig}\big(\delta_{Pj}-\delta_{Pi}\big)^{m/n}\Bigg)\cdot \tag{18}$$

Theorem 1: The bounded control input designed in (13) and (15) solves the fixed-time frequency restoration and active power-sharing problem in (3) and (4) simultaneously, with convergence time T_F given in (30).

Proof: Choose a candidate Lyapunov function as

$$V(t) = V_{\omega}(\boldsymbol{\delta_{\omega}}) + V_P(\boldsymbol{\delta_P}) = \frac{1}{2}\boldsymbol{\delta_{\omega}^T M_{\omega}\delta_{\omega}} + \frac{1}{2}\boldsymbol{\delta_P^T M_P\delta_P} \tag{19}$$

where $\boldsymbol{\delta_{\omega}} = [\delta_{\omega 1}, \delta_{\omega 2}, \ldots\delta_{\omega N}]^T$, $\boldsymbol{\delta_P} = [\delta_{P1}, \delta_{P2}, \ldots\delta_{PN}]^T$,

$$\boldsymbol{M_{\omega}} = \mathrm{diag}\Big\{\frac{1}{C_{\omega 1}}, \ldots, \frac{1}{C_{\omega N}}\Big\}, \quad \text{and}$$
$$\boldsymbol{M_P} = \mathrm{diag}\Big\{\frac{1}{C_{P1}}, \ldots, \frac{1}{C_{PN}}\Big\}.$$

Differentiating (19) with respect to time yields

$$\dot{V}(t) = \dot{V}_{\boldsymbol{\omega}}(\boldsymbol{\delta_{\omega}}) + \dot{V}_P(\boldsymbol{\delta_P}) = \boldsymbol{\delta_{\omega}^T M_{\omega}\dot{\delta}_{\omega}} + \boldsymbol{\delta_P^T M_P\dot{\delta}_P}\cdot \tag{20}$$

Substituting (17) and (18) in (20) yields,

$$\begin{aligned}\dot{V}(t) &= \sum_{i=1}^{N}\delta_{\omega i}\Bigg[\sum_{j\in\mathcal{N}_i}\alpha_{\omega}a_{ij}\mathrm{sig}\big(\delta_{\omega j}-\delta_{\omega i}\big)^{m/n} - \beta_{\omega}g_i\mathrm{sig}(\delta_{\omega i})^{m/n}\Bigg] + \sum_{i=1}^{N}\delta_{Pi}\Bigg[\sum_{j\in\mathcal{N}_i}\alpha_{P}a_{ij}\mathrm{sig}\big(\delta_{Pj}-\delta_{Pi}\big)^{m/n}\Bigg]\\ &= \sum_{i=1}^{N}\delta_{\omega i}\sum_{j\in\mathcal{N}_i}\alpha_{\omega}a_{ij}\mathrm{sig}\big(\delta_{\omega j}-\delta_{\omega i}\big)^{m/n} - \sum_{i=1}^{N}\beta_{\omega}\delta_{\omega i}g_i\mathrm{sig}(\delta_{\omega i})^{m/n} + \sum_{i=1}^{N}\delta_{Pi}\sum_{j\in\mathcal{N}_i}\alpha_{P}a_{ij}\mathrm{sig}\big(\delta_{Pj}-\delta_{Pi}\big)^{m/n}\cdot\end{aligned} \tag{21}$$

Using Lemma 1 (21) can be rewritten as

$$\begin{aligned}\dot{V}(t) = &-\frac{1}{2}\sum_{i=1}^{N}\sum_{j\in\mathcal{N}_i}\alpha_{\omega}a_{ij}\big(\delta_{\omega j}-\delta_{\omega i}\big)\mathrm{sig}\big(\delta_{\omega j}-\delta_{\omega i}\big)^{m/n}\\ &-\sum_{i=1}^{N}\beta_{\omega}g_i\delta_{\omega i}\mathrm{sig}(\delta_{\omega i})^{m/n}\\ &-\frac{1}{2}\sum_{i=1}^{N}\sum_{j\in\mathcal{N}_i}\alpha_{P}a_{ij}\big(\delta_{Pj}-\delta_{Pi}\big)\mathrm{sig}\big(\delta_{Pj}-\delta_{Pi}\big)^{m/n}\cdot\end{aligned} \tag{22}$$

Since $x\mathrm{sig}(x)^a = |x|^{a+1}$, (22) can be modified as,

$$\begin{aligned}\dot{V}(t) = &-\frac{1}{2}\sum_{i=1}^{N}\sum_{j\in\mathcal{N}_i}\alpha_{\omega}a_{ij}\big|\delta_{\omega j}-\delta_{\omega i}\big|^{(m+n)/n} - \sum_{i=1}^{N}\beta_{\omega}g_i|\delta_{\omega i}|^{(m+n)/n}\\ &-\frac{1}{2}\sum_{i=1}^{N}\sum_{j\in\mathcal{N}_i}\alpha_{P}a_{ij}\big|\delta_{Pj}-\delta_{Pi}\big|^{(m+n)/n}\\ \le &-\frac{1}{2}\Bigg(\sum_{i=1}^{N}\sum_{j\in\mathcal{N}_i}\big(\alpha_{\omega}a_{ij}\big)^{2n/(m+n)}\big|\delta_{\omega j}-\delta_{\omega i}\big|^2 + \sum_{i=1}^{N}\big(2\beta_{\omega}g_i\big)^{2n/(m+n)}|\delta_{\omega i}|^2\Bigg)^{(m+n)/2n}\\ &-\frac{1}{2}\Bigg(\sum_{i=1}^{N}\sum_{j\in\mathcal{N}_i}\big(\alpha_{P}a_{ij}\big)^{2n/(m+n)}\big|\delta_{Pj}-\delta_{Pi}\big|^2\Bigg)^{(m+n)/2n}\cdot\end{aligned} \tag{23}$$

Now constructing the Laplacian matrix $\mathscr{L}^{\omega}$ and $\mathscr{L}^{P}$ and pinning gain matrix G^{ω} with entries l_{ij}^{ω}, l_{ij}^{P} and g_{ij}^{ω} as $\mathscr{L}^{\omega} = \big[l_{ij}^{\omega}\big]_{N\times N}$, $\mathscr{L}^{P} = \big[l_{ij}^{P}\big]_{N\times N}$, and $G^{\omega} = \big[g_{ij}^{\omega}\big]_{N\times N}$, where (see equation below). Then, (23) can be written as,

$$\begin{aligned}\dot{V}(t) \le &-\frac{1}{2}\Bigg(\sum_{i=1}^{N}\sum_{j\in\mathcal{N}_i}l_{ij}^{\omega}\big|\delta_{\omega j}-\delta_{\omega i}\big|^2 + \sum_{i=1}^{N}g_{ij}^{\omega}|\delta_{\omega i}|^2\Bigg)^{(m+n)/2n}\\ &-\frac{1}{2}\Bigg(\sum_{i=1}^{N}\sum_{j\in\mathcal{N}_i}l_{ij}^{P}\big|\delta_{Pj}-\delta_{Pi}\big|^2\Bigg)^{(m+n)/2n}\cdot\end{aligned} \tag{24}$$

Assume, $Z_{\mathscr{L}}^{\omega} = \sum_{i=1}^{N}\sum_{j\in\mathcal{N}_i}l_{ij}^{\omega}\big|\delta_{\omega j}-\delta_{\omega i}\big|^2 + \sum_{i=1}^{N}g_{ij}^{\omega}|\delta_{\omega i}|^2$ and $Z_{\mathscr{L}^{\omega}} = \sum_{i=1}^{N}\sum_{j\in\mathcal{N}_i}l_{ij}^{P}\big|\delta_{Pj}-\delta_{Pi}\big|^2$ or in compact form

$$\begin{aligned}Z_{\mathscr{L}^{\omega}}(\boldsymbol{\delta_{\omega}}) &= 2\boldsymbol{\delta_{\omega}^T}(\mathscr{L}^{\omega}+G^{\omega})\boldsymbol{\delta_{\omega}},\\ Z_{\mathscr{L}^{P}}(\boldsymbol{\delta_P}) &= 2\boldsymbol{\delta_P^T}\big(\mathscr{L}^{P}\big)\boldsymbol{\delta_P}\cdot\end{aligned} \tag{25}$$

Using Lemmas 2 and 3, (25) can be modified as,

$$\begin{aligned}Z_{\mathscr{L}^{\omega}}(\boldsymbol{\delta_{\omega}}) &\ge 2\lambda_1(\mathscr{L}^{\omega}+G^{\omega})\boldsymbol{\delta_{\omega}^T\delta_{\omega}},\\ Z_{\mathscr{L}^{P}}(\boldsymbol{\delta_P}) &\ge 2\lambda_2\big(\mathscr{L}^{P}\big)\boldsymbol{\delta_P^T\delta_P}\cdot\end{aligned} \tag{26}$$

Now using (25), (24) can be rewritten as,

$$l_{ij}^{\omega} = \begin{cases}-\big(\alpha_{\omega}a_{ij}\big)^{\frac{2n}{(m+n)}}, & j\in N\\ \sum_{j\in\mathcal{N}_i}\big(\alpha_{\omega}a_{ij}\big)^{\frac{2n}{(m+n)}}, & j=i\end{cases}, \quad l_{ij}^{P} = \begin{cases}-\big(\alpha_{P}a_{ij}\big)^{\frac{2n}{(m+n)}}, & j\in N\\ \sum_{j\in\mathcal{N}_i}\big(\alpha_{P}a_{ij}\big)^{\frac{2n}{(m+n)}}, & j=i\end{cases},$$

and

$$g_{ij}^{\omega} = \begin{cases}\frac{1}{2}(2\beta_{\omega}g_i)^{\frac{2n}{(m+n)}}, & j=i\\ 0, & \text{otherwise}\end{cases}.$$

$$\dot{V}(t) \le -\frac{1}{2}(Z_{\mathscr{L}^\omega})^{\frac{m+n}{2n}} - \frac{1}{2}(Z_{\mathscr{L}^P})^{\frac{m+n}{2n}} \le -\frac{1}{2}\left(\frac{Z_{\mathscr{L}^\omega}}{V_\omega}\cdot V_\omega\right)^{\frac{m+n}{2n}} - \frac{1}{2}\left(\frac{Z_{\mathscr{L}^P}}{V_P}\cdot V_P\right)^{\frac{m+n}{2n}}. \quad (27)$$

Using (26) and (20), (27) can be written as

$$\dot{V}(t) \le -\frac{1}{2}\left(\frac{4\lambda_1(\mathscr{L}^\omega + G^\omega)\boldsymbol{\delta}_{\boldsymbol{\omega}}^{\boldsymbol{T}}\boldsymbol{\delta}_{\boldsymbol{\omega}}}{\boldsymbol{\delta}_{\boldsymbol{\omega}}^{\boldsymbol{T}}\boldsymbol{M}_{\boldsymbol{\omega}}\boldsymbol{\delta}_{\boldsymbol{\omega}}}\cdot V_\omega\right)^{\frac{m+n}{2n}} - \frac{1}{2}\left(\frac{4\lambda_2(\mathscr{L}^P)\boldsymbol{\delta}_{\boldsymbol{P}}^{\boldsymbol{T}}\boldsymbol{\delta}_{\boldsymbol{P}}}{\boldsymbol{\delta}_{\boldsymbol{P}}^{\boldsymbol{T}}\boldsymbol{M}_{\boldsymbol{P}}\boldsymbol{\delta}_P}\cdot V_P\right)^{\frac{m+n}{2n}} \le -\frac{1}{2}(4C_{\omega\min}\lambda_1(\mathscr{L}^\omega + G^\omega)\cdot V_\omega)^{\frac{m+n}{2n}} - \frac{1}{2}\left(4C_{P\min}\lambda_2(\mathscr{L}^P)\cdot V_P\right)^{\frac{m+n}{2n}}. \quad (28)$$

Defining $\eta_\omega = (1/2)(4C_{\omega\min}\lambda_1(\mathscr{L}^\omega + G^\omega))^{(m+n)/2n}$ and $\eta_P = (1/2)\left(4C_{P\min}\lambda_2(\mathscr{L}^P)\right)^{(m+n)/2n}$, where

$$C_{\omega\min} = \min\{C_{\omega 1}, \ldots, C_{\omega N}\},$$

(28) can be rewritten as

$$\dot{V}(t) = -\eta_\omega\cdot(V_\omega)^{(m+n)/2n} - \eta_P\cdot(V_P)^{(m+n)/2n}. \quad (29)$$

Thus, from Lemma 4, we can see that the Lyapunov function in (20) reaches zero in fixed-time given as,

$$T_f \le \frac{2n(V_\omega(0))^{\frac{m+n}{2n}}}{\eta_\omega(n-m)}, T_P \le \frac{2n(V_P(0))^{\frac{m+n}{2n}}}{\eta_P(n-m)}, \quad T_F \le \max\{T_f, T_P\}. \quad (30)$$

For any initial state $V(t) = 0, \forall t \ge T_F$. Therefore, the distributed, bounded, fixed-time frequency and active power regulation problem in (3) and (4) are solved at T_F.

This completes the proof. □

Remark 1: Simple implementation of fixed-time secondary control in (13) may result in disturbed active power sharing [25]. To provide accurate active power-sharing and faster convergence, we designed the fixed-time active power auxiliary control in (15).

Remark 2: The auxiliary control input for frequency and active power designed in (13) and (15) exploits the tracking error $\delta_{\omega i}$ and δ_{Pi}. This allows each DG to share information of angular frequency and active power (ω_j and $k_{Pj}^{\omega}P_j$, $j \in \mathscr{N}_i$) with neighbours in a distributed manner. The adjacent but not global information-sharing requirement can be fulfilled via sparse communication network with low communication cost.

Remark 3: From (30), it is clear that the upper bound of the settling time T_F only depends on the controller design specification m, n, α_ω, β_ω, initial values, and connectivity of the communication network i.e. smallest eigenvalue of matrix $(\mathscr{L}^\omega + G^\omega)$ and second smallest eigenvalue of $\mathscr{L}^P$. As a result, desired convergence time can be tuned via setting the controller gains.

Remark 4: The proposed distributed and fixed-time control protocols in (13) and (15) are equipped with bounded control input constraints, which can greatly suppress the transient and desirable for practical applications.

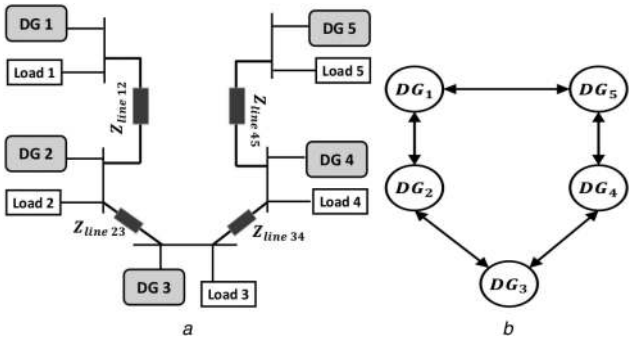

Fig. 3 *MG test system*
(a) Single line diagram of islanded MG test system,
(b) Communication topology

Table 1 Parameters of the proposed algorithm

Frequency controller	Voltage controller	Reference
$\alpha_\omega = 20, \alpha_P = 20$	$\alpha_V = 10$	$V_{\text{nom}} = 380\,\text{V}$
$\beta_\omega = 8$	$\beta_V = 4$	$f_{\text{nom}} = 50\,\text{Hz}$
$m = 1, n = 9,$	$m = 1, n = 9$	$\omega_{\text{nom}} = 314.16\,\text{rad/s}$

3.2 Voltage regulation

The distributed, fixed-time auxiliary secondary voltage restoration scheme with a bounded control input ξ_i^V is designed as

$$\xi_i^V = C_{Vi}\left(\sum_{j\in\mathscr{N}_i}\alpha_V a_{ij}\text{sig}(V_j - V_i)^{m/n} + \beta_V g_i\text{sig}(V_{\text{ref}} - V_i)^{m/n}\right) \quad (31)$$

where C_{vi} is positive gain satisfying following inequality

$$0 < C_{Vi} \le \frac{B_{Vi}}{|g_i| + \sum_{j\in\mathscr{N}_i}|a_{ij}|} \quad (32)$$

with $B_{Vi} > 0$ is the upper bound of the control input ξ_i^V; $\mathscr{N}_i$ is the set of neighbours; V_{ref} is the voltage reference; m, n are odd positive integers with $m < n$ and α_V, β_V are coupling gains.

Theorem 2: The bounded control input designed in (31) guarantees the synchronisation of DGs output voltage with reference voltage within fixed convergence time

$$T_V \le \frac{2n(V_V(0))^{(m+n)/2n}}{\eta_V(n-m)},$$

where

$$\eta_V = \frac{1}{2}\left(4C_{V\min}\lambda_1(\mathscr{L}^V + G^V)\right)^{(m+n)/2n}, \quad \text{and}$$
$$C_{V\min} = \min\{C_{V1}, \ldots, C_{VN}\}.$$

Proof: : The proof is similar to the proof of Theorem 1.

4 Case studies

In this section, a 380 V/50 Hz islanded MG test system is simulated in MATLAB/SimPowerSystem environment. Fig. 3*a* shows the single line block diagram consists of DGs, five loads, four lines. Fig. 3*b* shows the communication topology. The detailed specifications of the parameters of MG, loads, and the proposed controller are given in Tables 1–3, respectively. The associated Laplacian matrix for graph shown in Fig. 3*b* is designed as follows. $\mathscr{L} = [2, -1, 0, 0, -1; -1, 2, -1, 0, 0; 0, -1, 2, -1, 0; 0, 0, -1, 2, -1; -1, 0, 0, -1, 2]$.

Table 2 Specification of MG test system

DG 1 & DG 2 & DG 3		DG 4 & DG 5	
DGs			
k_Q^V	9.4×10^{-5}	k_Q^V	12.5×10^{-5}
k_P^ω	1.3×10^{-3}	k_P^ω	1.5×10^{-3}
R	0.03 Ω	R	0.03 Ω
L	0.35 mH	L	0.35 mH
R_f	0.1 Ω	R_f	0.1 Ω
L_f	1.35 mH	L_f	1.35 mH
C_f	50 μF	C_f	50 μF
K_{PV}	0.1	K_{PV}	0.05
K_{IV}	420	K_{IV}	390
K_{PC}	15	K_{PC}	10.5
K_{IC}	20,000	K_{IC}	16,000
lines			
Z_{Line12}	Z_{Line23}	Z_{Line34}	Z_{Line45}
$R_l = 0.12\,\Omega$	$R_l = 0.175\,\Omega$	$R_l = 0.12\,\Omega$	$R_l = 0.175\,\Omega$
$L_l = 318\,\mu\text{H}$	$L_l = 1847\,\mu\text{H}$	$L_l = 318\,\mu\text{H}$	$L_l = 1847\,\mu\text{H}$

Table 3 MG loads

Load 1	Load 2	Load 3	Load 4	Load 5
loads				
$R = 300\,\Omega$	$R = 40\,\Omega$	$R = 50\,\Omega$	$R = 40\,\Omega$	$R = 50\,\Omega$
$L = 477$ mH	$L = 64$ mH	$L = 64$ mH	$L = 64$ mH	$L = 95$ mH

The leader adjacency matrix can be designed as $G = \text{diag}[1, 0, 0, 0]$ considering that the DG 1 has access to the reference values.

4.1 Effect of load perturbation

This case explains the transient performance of the proposed control scheme for an MG islanded at $t = 0$ s. At the beginning, only primary control was active for the time interval (0.0 s–2 s), as shown in Fig. 4. Voltage and frequency deviations can be seen at $t = 1$ s and $t = 1.5$ s, when loads are suddenly connected to MG network. This clearly shows that the active droop-based primary control scheme stabilises the voltage magnitude and operating frequency, but unable to restore them to their nominal values. Next, at $t = 2$ s, the proposed secondary control schemes in (13), (15), and (31) are activated. The voltage and frequency deviations caused by the primary control scheme are eliminated within 0.24 s and restored to their nominal values. Further, to evaluate the controller performance under load disturbance, an additional RL load of $R = 30\,\Omega, L = 47$ mH is attached to DG3 at $t = 3$ s and disconnected at $t = 4$ s. Figs. 4*a*–*c* show that the proposed control scheme exhibits good tracking and robust performance against the inclusion of RL load and restores the DG voltage and frequency within 0.25 and 0.26 s, respectively, while sharing active power accurately. Further, by disconnecting the load at $t = 4$ s, results in voltage and frequency deviations from the nominal values. However, the proposed secondary control scheme restores the voltage and frequency in 0.25 and 0.24 s, respectively. From Fig. 4*b*, it can be observed that the maximum frequency deviation is up to 49.96 Hz which is within an acceptable limit of maximum frequency deviation of 0.5 Hz according to 'IEEE standard for Interconnecting Distributed Resources with Electric Power System Amendment 1' [22]. It can be seen from Fig. 4*d* that the reactive power-sharing of DGs shows some discrepancies. It is because of the line impedance effect. The control inputs of the proposed control scheme are bounded and becomes zero when the consensus is achieved. The corresponding frequency control input is shown in Fig. 5.

Next, to verify the performance of the proposed control scheme during fast changing operating condition, a time varying load of $R = 15\,\Omega, L = 20$ mH is connected at $t = 6.0$ s, and it doubles every 2 s. Fig. 6 shows the operating frequency of DGs under time varying load. The results show that the frequency variations are eliminated by the secondary control in fixed-time duration and frequency for all DGs are well regulated to their nominal values.

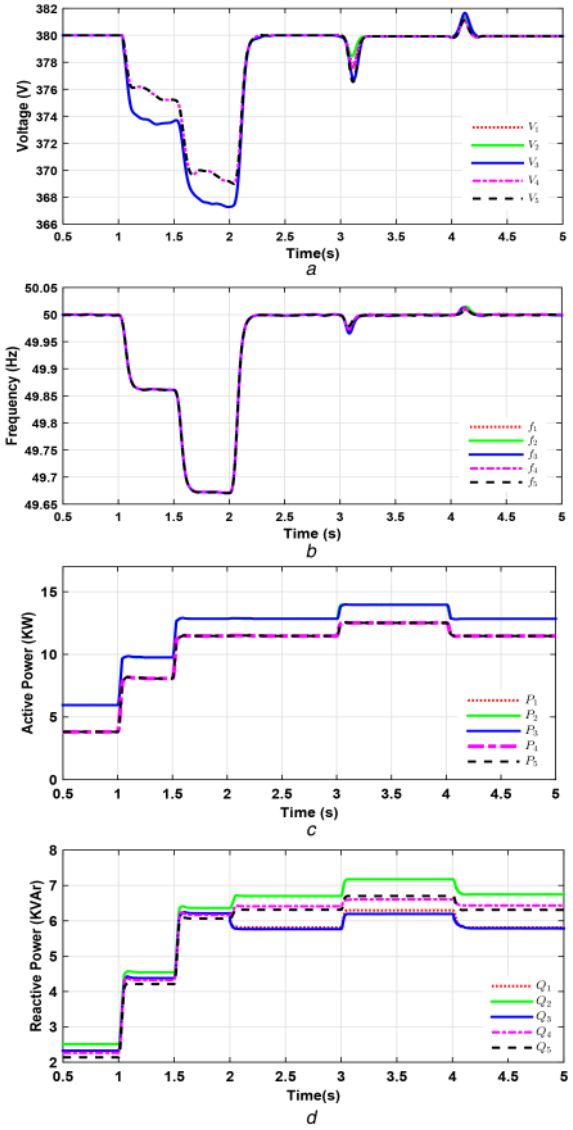

Fig. 4 *Performance under load perturbation*
(a) DG output voltage magnitude,
(b) DG frequency,
(c) DG output active power,
(d) DG output reactive power

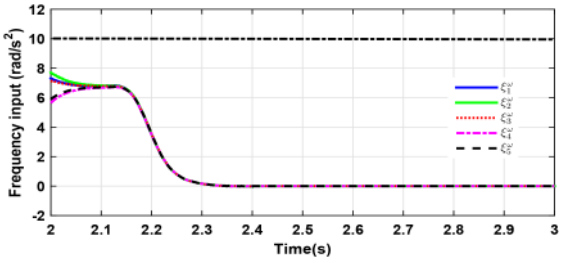

Fig. 5 *Auxiliary frequency control input under the proposed control strategy for time span of 2.0 s–3.0 s*

4.2 Influence of DG plug-and-play

In this case, the performance of the proposed controller is verified for the plug-and-play (PNP) operation. The DG units keep moving in and out from the MG network due the continuously changing nature of RES. It is a common contingency and it demands for PNP support from the controller unit. The proposed fixed-time bounded

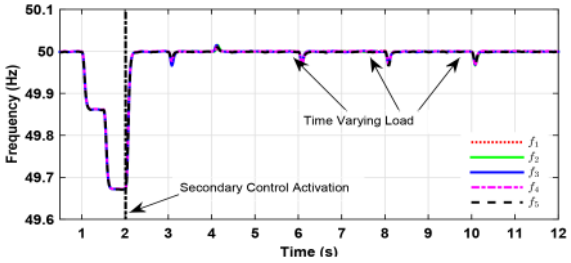

Fig. 6 *DG's operating frequency under time-varying load*

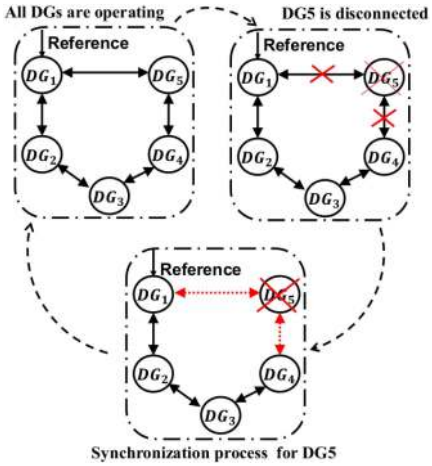

Fig. 7 *Communication graph configuration under PNP operation*

input controller facilitates the plug and play operation seamlessly. To show this, DG 5 is disconnected at $t = 3$ s, resulting in communication link 4–5 breakage. However, the remaining DGs still form the connecting graph shown in Fig. 7. The proposed secondary control schemes are active, and the results in Fig. 8 show that the disconnection of DG 5 results in power imbalance. The active power and reactive power outputs of DG 5 drop to zero slowly because of the output low-pass filter, while the power deficiency is reassigned among the remaining DG units. The drop in output power of DG 5 causes its operation voltage and frequency to increase slightly. However, as the secondary control scheme is active, the operating voltage and frequency of all DGs are well-regulated despite the transients caused by DG 5 disconnection. Next, at $t = 4$ s, DG 5 is connected to the MG network. The communication graph is revised and modified as shown in Fig. 7. Simulation results show that the voltage, frequency, and active powers regulation are maintained effectively with minimal transients at disconnection/connection points.

4.3 Influence of different communication topologies

In this case, the proposed controller performance is analysed under ring-, line-, and mesh-shaped topologies (Fig. 9). The convergence time of the proposed controller depends on the spectral radius of the graph, which denotes the connectivity of the communication network, and it varies with different communication topologies. The change of communication topology results in different communication diagraph, and hence the Laplacian matrix is changed accordingly. Therefore, for different Laplacian matrix, the second smallest eigenvalues (spectral radius) are different and hence the corresponding convergence times are different as given in Table 4. However, for the proposed fixed-time voltage, frequency, and power regulation scheme, the restoration time is not significantly varying for above-mentioned topologies as given in Table 4 due to less number of DG units in the test MG system. Further, Fig. 10 shows the performance of the proposed control scheme under radial topology. The control scheme accurately restores the voltage and frequency to their nominal values and active and reactive powers are shared according to their droop gains with change in communication topology. Hence, our

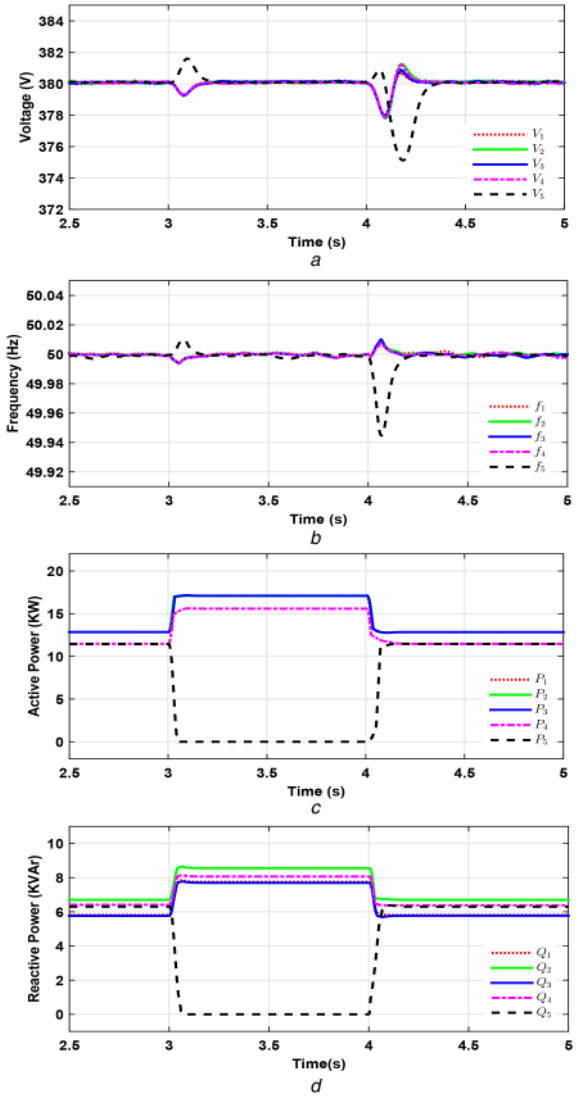

Fig. 8 *Performance under plug-and-play operation*
(a) DG output voltage magnitude,
(b) DG frequency,
(c) DG output active power,
(d) DG output reactive power

proposed control scheme works appropriately with different communication topologies.

4.4 Comparative performance evaluation

A few studies in [12, 15, 17] consider the same problem of voltage and frequency synchronisation using asymptotic control approaches. The proposed finite-time bounded input control schemes restores the voltage and frequency and shares the active power accurately in fixed time interval. To analyse the convergence performance, a comparison between the proposed distributed bounded fixed-time controller and the traditional control approach in [12] is presented. Fig. 11 shows that the proposed control scheme achieves consensus rapidly and exhibits robust and faster convergence performance under controller activation and load perturbation. The proposed control scheme restores the voltage in ∼0.22 s, whereas the conventional controller in [12] restores the voltage in 0.35 s. Similarly the proposed controller restore the frequency in ∼0.18 s and the conventional controller in [12] restores the frequency in 0.3 s. Fig. 12 shows the frequency control input for the frequency restoration scheme presented in [12]. It is clear from Fig. 12 that the frequency control input shows more transient overshoot and exceeds the boundary and hence results in more transients as compared to the frequency control input for the proposed controller shown in Fig. 5.

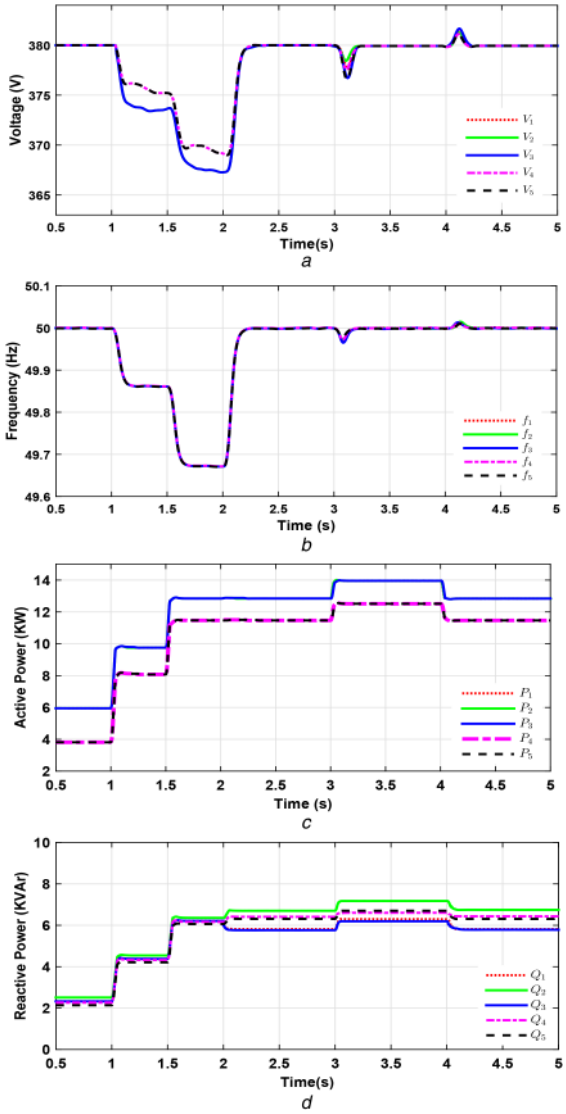

Fig. 9 *Performance under radial communication topology*
(a) DG output voltage magnitude,
(b) DG frequency,
(c) DG output active power,
(d) DG output reactive power

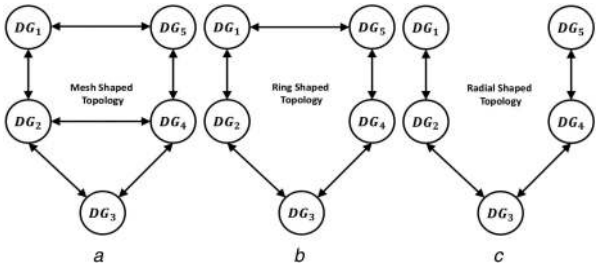

Fig. 10 *Different Communication topologies for case 4.3*
(a) Mesh,
(b) Ring,
(c) Radial

4.5 Comparison with control scheme in [20]

In the literature, several studies reported that deal with both the voltage and frequency synchronisation in distributed manner [18–22]. The work in [20] considered the similar control problems. Therefore, we compare the proposed fixed-time controller with the controller reported in [20] for the same MG test system shown in Fig. 3. Fig. 13 shows that the proposed bounded control scheme outperforms the control approach reported in [20]. Our proposed control scheme exhibit faster convergence for controller activation and load variations as compared to the control scheme reported in [20].

Table 4 Convergence time for different communication topologies

Topology	Mesh	Ring	Radial
spectral radius	2.4812	2	1.7321
convergence time	0.22 s	0.23 s	0.26 s

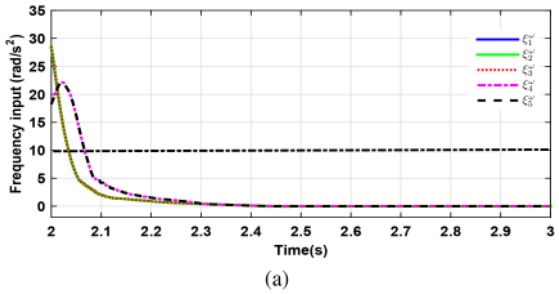

Fig. 11 *Auxiliary frequency control input under linear consensus control strategy in [12]*
(a) DG output voltage magnitude,
(b) DG frequency

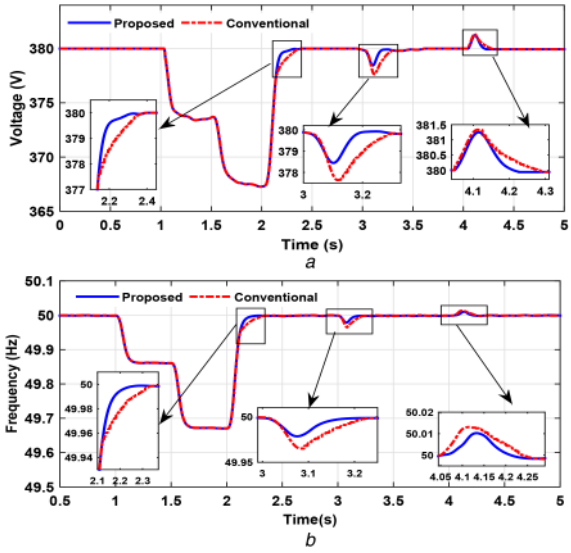

Fig. 12 *Performance comparison with method in [12] for time span of 2.0 s–3.0 s*
(a) DG output voltage magnitude,
(b) DG frequency

5 Conclusion

This paper address the problem of voltage and frequency restoration in an islanded MG network. A distributed fixed-time secondary control scheme with constrained control input is proposed for both voltage and frequency synchronisation and accurate active power-sharing among the DG units. The proposed control scheme restores the voltage and frequency of DG unit in finite-time, while satisfying the bounded input constraint, and keeping the control inputs within the limits. Therefore, it reduces the transient overshoots in voltage and frequency output of DG unit. Further, the upper bound on the convergence time is established using the Lyapunov theory. The obtained settling time is independent of MG system parameters such as lines and loads. However, it depends on the connectivity of the communication network. The convergence time analysis is provided for different type of communication topologies to clearly show the effect of change in communication topology. Compared to the conventional approach, the proposed control scheme exhibits faster convergence and better small signal (load perturbation) and large signal (loss of

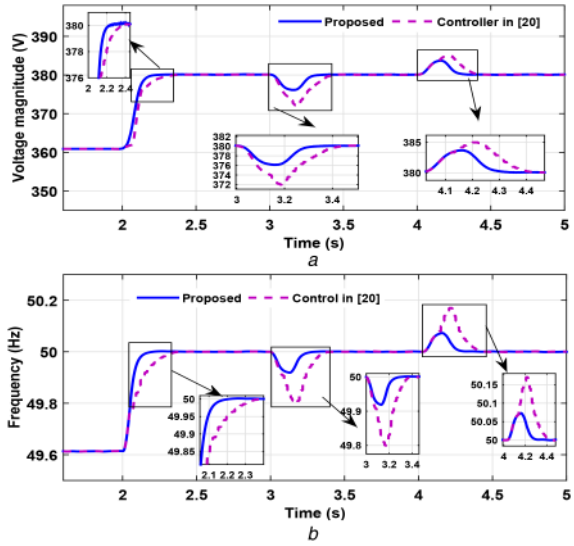

Fig. 13 *Performance comparison with method in [20]*
(a) DG output voltage magnitude,
(b) DG frequency

DG unit) disturbance rejection. The proposed control schemes are fully distributed and can be implemented on a low-cost sparse communication network. Also, the proposed control scheme supports the plug and play feature of MG network.

6 References

[1] Abbott, D.: 'Keeping the energy debate clean: How do we supply the world's energy needs?', *Proc. IEEE*, 2010, **98**, (1), pp. 42–66

[2] Lasseter, R.H.: 'Microgrids and distributed generation', *J. Energy Eng.*, 2007, **133**, (3), pp. 144–149

[3] Katiraei, F., Iravani, M.R., Lehn, P.W.: 'Micro-grid autonomous operation during and subsequent to islanding process', *IEEE Trans. Power Deliv.*, 2005, **20**, (1), pp. 248–257

[4] Lopes, J.P., Moreira, C., Madureira, A.: 'Defining control strategies for microgrids islanded operation', *IEEE Trans. Power Syst.*, 2006, **21**, (2), pp. 916–924

[5] Guerrero, J.M., Chandorkar, M., Lee, T.L., *et al.*: 'Advanced control architectures for intelligent microgrids – part I: decentralized and hierarchical control', *IEEE Trans. Ind. Electron.*, 2013, **60**, (4), pp. 1254–1262

[6] Bidram, A., Davoudi, A.: 'Hierarchical structure of microgrids control system', *IEEE Trans. Smart Grid*, 2012, **3**, (4), pp. 1963–1976

[7] Guerrero, J.M., Vasquez, J.C., Matas, J., *et al.*: 'Hierarchical control of droop-controlled AC and DC microgrids – A general approach toward standardization', *IEEE Trans. Ind. Electron.*, 2011, **58**, (1), pp. 158–172

[8] Vovos, P.N., Kiprakis, A.E., Wallace, A.R., *et al.*: 'Centralized and distributed voltage control: impact on distributed generation penetration', *IEEE Trans. Power Syst.*, 2007, **22**, (1), pp. 476–483

[9] Tan, K., Peng, X., So, P.L., *et al.*: 'Centralized control for parallel operation of distributed generation inverters in microgrids', *IEEE Trans. Smart Grid*, 2012, **3**, (4), pp. 1977–1987

[10] Liu, W., Gu, W., Sheng, W., *et al.*: 'Decentralized multi-agent system-based cooperative frequency control for autonomous microgrids with communication constraints', *IEEE Trans. Sustain. Energy*, 2014, **5**, (2), pp. 446–456

[11] Olivares, D.E., Mehrizi-Sani, A., Etemadi, A.H., *et al.*: 'Trends in microgrid control', *IEEE Trans. Smart Grid*, 2014, **5**, (4), pp. 1905–1919

[12] Bidram, A., Davoudi, A., Lewis, F.L., *et al.*: 'Secondary control of microgrids based on distributed cooperative control of multi-agent systems', *IET Gener. Transm. Distrib.*, 2013, **7**, (8), pp. 822–831

[13] Bidram, A., Davoudi, A., Lewis, F.L., *et al.*: 'Distributed cooperative secondary control of microgrids using feedback linearization', *IEEE Trans. Power Syst.*, 2013, **28**, (3), pp. 3462–3470

[14] Simpson-Porco, J.W., Shafiee, Q., Dorfler, F., *et al.*: 'Secondary frequency and voltage control of islanded microgrids via distributed averaging', *IEEE Trans. Ind. Electron.*, 2015, **62**, (11), pp. 7025–7038

[15] Shafiee, Q., Guerrero, J.M., Vasquez, J.C.: 'Distributed secondary control for islanded microgrids – a novel approach', *IEEE Trans. Power Electron.*, 2014, **29**, (2), pp. 1018–1031

[16] Nasirian, V., Shafiee, Q., Guerrero, J.M., *et al.*: 'Droop-free distributed control for AC microgrids', *IEEE Trans. Power Electron.*, 2016, **31**, (2), pp. 1600–1617

[17] Shrivastava, S., Subudhi, B., Das, S.: 'Distributed voltage and frequency synchronisation control scheme for islanded inverter-based microgrid', *IET Smart Grid*, 2018, **1**, (2), pp. 48–56

[18] Bidram, A., Davoudi, A., Lewis, F.L.: 'Finite-time frequency synchronization in microgrids'. 2014 IEEE Energy Conversion Congress and Exposition (ECCE), PA, USA, 2014, pp. 2648–2654

[19] Cady, S.T., Dominguez-Garcia, A.D., Hadjicostis, C.N.: 'Finite-time approximate consensus and its application to distributed frequency regulation in islanded ac microgrids'. IEEE 2015 48th Hawaii Int. Conf. on System Sciences (HICSS), Kauai, USA, 2015, pp. 2664–2670

[20] Guo, F., Wen, C., Mao, J., *et al.*: 'Distributed secondary voltage and frequency restoration control of droop-controlled inverter-based microgrids', *IEEE Trans. Ind. Electron.*, 2015, **62**, (7), pp. 4355–4364

[21] Lou, G., Gu, W., Xu, Y., *et al.*: 'Distributed MPC-based secondary voltage control scheme for autonomous droop-controlled microgrids', *IEEE Trans. Sustain. Energy*, 2017, **8**, (2), pp. 792–804

[22] : 'IEEE standard conformance test procedures for equipment interconnecting distributed resources with electric power systems - amendment 1'. IEEE Std 15471a-2015 (Amendment to IEEE Std 15471-2005), 2015, pp. 1–27

[23] Dehkordi, N.M., Sadati, N., Hamzeh, M.: 'Distributed robust finite-time secondary voltage and frequency control of islanded microgrids', *IEEE Trans. Power Syst.*, 2017, **32**, (5), pp. 3648–3659

[24] Wang, X., Zhang, H., Li, C.: 'Distributed finite-time cooperative control of droop-controlled microgrids under switching topology', *IET Renew. Power Gener.*, 2017, **11**, (5), pp. 707–714

[25] Lu, X., Yu, X., Lai, J., *et al.*: 'A novel distributed secondary coordination control approach for islanded microgrids', *IEEE Trans. Smart Grid*, 2018, **9**, (4), pp. 2726–2740

[26] Deng, Z., Xu, Y., Sun, H., *et al.*: 'Distributed, bounded and finite-time convergence secondary frequency control in an autonomous microgrid', *IEEE Trans. Smart Grid*, 2018, doi: 10.1109/TSG.2018.2810287, to appear

[27] Pogaku, N., Prodanovic, M., Green, T.C.: 'Modeling, analysis and testing of autonomous operation of an inverter-based microgrid', *IEEE Trans. Power Electron.*, 2007, **22**, (2), pp. 613–625

[28] Zuo, S., Davoudi, A., Song, Y., *et al.*: 'Distributed finite-time voltage and frequency restoration in islanded AC microgrids', *IEEE Trans. Ind. Electron.*, 2016, **63**, (10), pp. 5988–5997

[29] Zhang, H., Lewis, F.L., Qu, Z.: 'Lyapunov, adaptive, and optimal design techniques for cooperative systems on directed communication graphs', *IEEE Trans. Ind. Electron.*, 2012, **59**, (7), pp. 3026–3041

[30] Bhat, S.P., Bernstein, D.S.: 'Continuous finite-time stabilization of the translational and rotational double integrators', *IEEE Trans. Autom. Control*, 1998, **43**, (5), pp. 678–682